# Dynamic Block-Based Parameter Estimation for MRF Classification of High-Resolution Images

Hossein Aghighi, John Trinder, Yuliya Tarabalka, Samsung Lim

▶ **To cite this version:**

Hossein Aghighi, John Trinder, Yuliya Tarabalka, Samsung Lim. Dynamic Block-Based Parameter Estimation for MRF Classification of High-Resolution Images. IEEE Geoscience and Remote Sensing Letters, 2014, 11 (10), pp.1687-1691. hal-01016505

**HAL Id: hal-01016505**
**https://inria.hal.science/hal-01016505**

Submitted on 30 Jun 2014

**HAL** is a multi-disciplinary open access archive for the deposit and dissemination of scientific research documents, whether they are published or not. The documents may come from teaching and research institutions in France or abroad, or from public or private research centers.

L'archive ouverte pluridisciplinaire **HAL**, est destinée au dépôt et à la diffusion de documents scientifiques de niveau recherche, publiés ou non, émanant des établissements d'enseignement et de recherche français ou étrangers, des laboratoires publics ou privés.

# Dynamic Block-Based Parameter Estimation for MRF Classification of High-Resolution Images

Hossein Aghighi, *Student Member, IEEE*, John Trinder, Yuliya Tarabalka, *Member, IEEE*, and Samsung Lim

***Abstract*—A Markov random field is a graphical model that is commonly used to combine spectral information and spatial context into image classification problems. The contributions of the spatial versus spectral energies are typically defined by using a smoothing parameter, which is often set empirically. We propose a new framework to estimate the smoothing parameter. For this purpose, we introduce the new concepts of dynamic blocks and class label cooccurrence matrices. The estimation is then based on the analysis of the balance of spatial and spectral energies computed using the spatial class co-occurrence distribution and dynamic blocks. Moreover, we construct a new spatially weighted parameter to preserve the edges, based on the Canny edge detector. We evaluate the performance of the proposed method on three data sets: a multispectral DigitalGlobe WorldView-2 and two hyperspectral images, recorded by the AVIRIS and the ROSIS sensors, respectively. The experimental results show that the proposed method succeeds in estimating the optimal smoothing parameter and yields higher classification accuracy values when compared with state-of-the-art methods.**

***Index Terms*—Classification, Markov random field (MRF), smoothing parameter, support vector machine (SVM).**

## I. Introduction

THE latest and upcoming generations of optical imaging sensors capture data with very high spectral and spatial resolutions. This raises new opportunities for remote sensing applications and challenges, where both spectral and spatial image contents have to be analyzed. Markov random fields (MRFs) are probabilistic models that are commonly used to incorporate spatial information via a neighborhood system for image classification problems [1]. In the MRF framework, the maximum *a posteriori* (MAP) decision rule is commonly formulated as the minimization of an energy function comprising spatial and spectral terms. One of the theoretical challenges consists in the proper choice of the balance between the contributions of these two energy terms, which is controlled by a weight or a *smoothing parameter*. It has been demonstrated that a too large value of the smoothing parameter results in oversmoothing of the classification map and that a too small value does not fully utilize the available spatial information [2].

In order to estimate the smoothing parameter, Derin and Elliott used the least squares approach in terms of a second-order neighborhood system [3]. Later on, several heuristic methods have been proposed to improve parameter estimation and classification accuracy, such as iterative conditional estimation [4], genetic algorithms [5], Ho–Kashyap optimization method [6], and simulated annealing [2]. Jia and Richards [7] used the normalization value of the spatial and spectral components in the range (0, 1) to determine weighting coefficient estimation.

Recently, Tolpekin and Stein [8] followed by Li *et al.* [2] have proposed to estimate the smoothing parameter based on the analysis of the local energy balance. They concluded that the smoothing parameter is affected by class separability, scale factor information, neighborhood system size, configuration of class labels, and choice of the power-law index. Although their method proposed an efficient way for estimating the smoothing weight, it introduced another parameter, which was set as the constant empirical value in [8] and [2]. Because this parameter depends on the configuration of class labels in the image, it can be estimated based on the spatial frequency distribution of each pair of classes in each specific image, what was not done in [8] and [2]. Moreover, the existing methods suffer from the equal-class covariance matrix assumption.

This letter presents a novel and robust framework for smoothing parameter estimation under the Gaussian class-conditional density assumption, which overcomes the limitations of the use of constant empirical values. A contextually adaptive smoothing parameter estimation method is proposed on the basis of the balance of spatial and spectral energies and the global spatial frequency distribution of co-occurrence class label. The class labels are estimated by introducing three new concepts called the dynamic blocks, class-label co-occurrence matrix of the blocks (CLCMB) and global class-label co-occurrence matrix of the blocks (GCLCMB), which comprise the second contribution of this letter. The third contribution of this letter is a new edge probability index to preserve the information and location of edges while performing spatial regularization.

The outline of this letter is as follows: Section II explains the framework of the proposed method and details of each step. In Section III, the data description and the experimental results are presented and discussed. Finally, conclusions are drawn in Section IV.

Manuscript received November 18, 2013; revised January 13, 2014; accepted February 3, 2014.

H. Aghighi is with the School of Civil and Environmental Engineering, The University of New South Wales, Sydney, NSW 2052, Australia and also with the Department of Remote Sensing and GIS, Faculty of Earth Science, Shahid Beheshti University, Tehran 1983963113, Iran (e-mail: h.aghighi@student.unsw.edu.au).

J. Trinder and S. Lim are with the School of Civil and Environmental Engineering, The University of New South Wales, Sydney, NSW 2052, Australia (e-mail: j.trinder@unsw.edu.au; s.lim@unsw.edu.au).

Y. Tarabalka is with the AYIN Research Team, Inria Sophia Antipolis Méditerranée, 06902 Sophia Antipolis, France (e-mail: yuliya.tarabalka@inria.fr).

Color versions of one or more of the figures in this paper are available online at http://ieeexplore.ieee.org.

Digital Object Identifier 10.1109/LGRS.2014.2305913

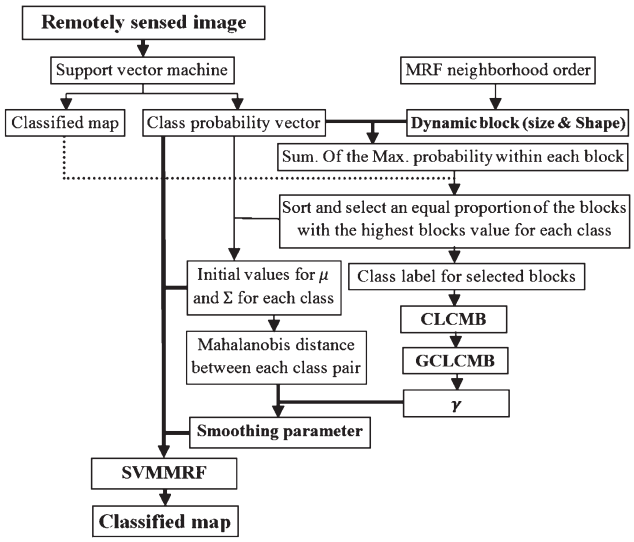


Fig. 1. Flowchart of the smoothing parameter estimation approach and the *SVMMRF* classification scheme.

## II. Material and Methods

The proposed MRF classification model and processing steps to estimate the smoothing parameter are presented in Fig. 1. We denote an image by $Y = \{y_i \in \mathbb{R}^B, i = 1, 2, \ldots, m\}$, where $B$ is a number of spectral channels, and $m$ is a number of pixels. Let $\Omega = \{\omega_1, \omega_2, \ldots, \omega_M\}$ be a set of $M$ thematic classes of interest. The classification task consists in assigning for each pixel $y_j$ a class label $\ell_j$, yielding the classification map $\mathbf{l} = \{\ell_j, j = 1, 2, \ldots, m\}$.

### A. Potts MRF model

The basic concept of an MRF is that the neighboring labels have a direct interaction with each other, and neighboring pixels belong with high probability to the same class [9]. In this research, the expectation–maximization algorithm [10] is adopted for computing the MAP, which optimizes the global energy function in the image by minimizing the local posterior energies, i.e.,

$$U(y_i) = \lambda U_{\text{spatial}}(y_i) + (1 - \lambda) U_{\text{spectral}}(y_i) \tag{1}$$

where $\lambda$ is the smoothing parameter, $U_{\text{spectral}}(y_i)$ is the spectral energy function in MRF, and $U_{\text{spatial}}(y_i)$ is the spatial energy term computed over neighborhood $(N_i)$ of pixel $y_i$. We define the spectral energy term as [9]

$$U_{\text{spectral}}(y_i) = -\ln\{P(y_i|\ell_i)\} \tag{2}$$

where $P(y_i|\ell_i)$ is estimated by pairwise coupling of probability estimates from "one versus one" support vector machine (SVM) outputs. The spatial energy term is defined by the Potts model, which penalizes a pair of different class labels for neighboring pixels, i.e.,

$$U^{\text{NE}}_{\text{spatial}}(y_i) = \sum_{y_j \in \mathbf{N}_i} (1 - \delta(\ell_i, \ell_j)) \tag{3}$$

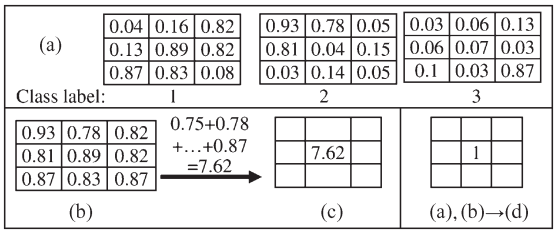


Fig. 2. Procedure for applying a dynamic block to the SVM probability estimations and results of each step. (It is assumed that the original image has three classes.) (a) SVM probability in a specific block for each class. (b) Selection of maximum class probabilities in that block. (c) Summation of the selected probability in that block. (d) Block class label based on the probability of the central pixel class label.

where $N_i$ defines a symmetric neighborhood for pixel $y_i$, and $\delta(\ell_i, \ell_j)$ is the Kronecker delta function $\delta(\ell_i, \ell_j) = 1$ if $\ell_i = \ell_j$ and $\delta(\ell_i, \ell_j) = 0$ if $\ell_i \neq \ell_j$. The superscript NE means that no edge information is used [9].

### B. Smoothing Parameter Estimation

Assume that a pixel $i$ with the true label $\ell_i = \alpha$ is assigned to an incorrect class label $\ell_i = \beta$. The change from $\alpha$ to $\beta$ leads to a change in the local likelihood energy $\Delta U^l_{\alpha\beta}$, which is equal to the Mahalanobis distance between two classes, and a change in the local prior energy, which is simplified as $\Delta U^P_{\alpha\beta} = q\psi_{\alpha\beta}$ [8], where $q = \lambda/(1 - \lambda)$ controls the overall magnitude of the weights, and $\psi_{\alpha\beta}$ depends on the size of the neighborhood system and the configuration of class label $\ell_i$ in its neighborhood pixels [8]. Once $\Delta U^l_{\alpha\beta}$ and $\psi_{\alpha\beta}$ are computed, the smoothing parameter for a pair of classes can be estimated as follows [8]:

$$\lambda_{\alpha\beta} = \frac{1}{1 + \frac{\psi_{\alpha\beta}}{\Delta U^l_{\alpha\beta}}}. \tag{4}$$

In previous research, the value of $\psi_{\alpha\beta}$ is set as an empirical constant value, and $\Delta U^l_{\alpha\beta}$ is computed using an equal covariance matrix for all of the classes [2], [8]. This letter proposes a new robust adaptive method to estimate $\psi_{\alpha\beta}$, $\Delta U^l_{\alpha\beta}$, $\lambda_{\alpha\beta}$, and, consequently, $\lambda^*$, which is an optimum smoothing parameter for the image. For this purpose, we use the new concepts of dynamic blocks, CLCMB and GCLCMB described in the following sections. Moreover, we compute the average covariance for each pair of classes instead of using the same covariance matrix for all the classes [2], [8].

### C. Dynamic Block

A dynamic block is defined based on the neighborhood system, cliques, and the Markovianity concept in MRFs, where their shape and size correspond to the selected MRF neighborhood system [11]. In this research, we employ a second-order neighborhood system. Hence, the block shape is a square with a size of $3 \times 3$ pixels. A block should satisfy the following conditions: Each block reports one value, which is the summation of the maximum probabilities of neighbors within the block. Consequently, neighbors outside the block are ignored (see Fig. 2). The block is applied to the probability estimations derived from SVM outputs [see Fig. 2(a)], and each pixel of the block selects the maximum class probability of the relevant pixel [see

Fig. 2(b)]. Then, the sum of the selected values for each block is calculated and assigned to the central pixel in that block [see Fig. 2(c)]. In the next steps, the blocks are categorized based on the class labels of their central pixels [see Fig. 2(d)]. The blocks of each class are then sorted in descending order based on their probability sums [see Fig. 2(c)], and an equal proportion of blocks with the highest sums is selected for each class. These selected blocks are assumed to be reliably classified.

Next, the mean and covariance of each class are estimated using the SVM probability vectors for the central pixels of the selected blocks of each class. Then, the estimated means and covariances are used to compute $\Delta U^l_{\alpha\beta}$, i.e.,

$$\Delta U^l_{\alpha\beta} = \frac{1}{2}\left(\mu_\beta - \mu_\alpha\right)' \Sigma^{-1} \left(\mu_\beta - \mu_\alpha\right) \tag{5}$$

where $\Sigma$ is computed using the average of the covariances for each pair of classes instead of using the same covariance matrix for all the classes [8]. The final output of this step is a square matrix of size $M$, which shows the Mahalanobis distance for each pair of classes. Moreover, the class code of the pixels of the selected blocks is extracted and used to calculate the CLCMB and the GCLCMB (see Section II-D).

### D. CLCMB and GCLCMB

According to the concept of dynamic blocks, a new concept is defined and is called the class-label co-occurrence matrix of the blocks (CLCMB) [11]. CLCMB is a square matrix of size $M$ that provides information about the spatial frequency distribution of each pair of classes in the selected blocks of each class; a similar concept with a different methodology was introduced in [12]. Let $N_b$ be the number of selected blocks for a class $\omega_i$. Since the second-order neighboring system is chosen, each central pixel $(y_i)$ is surrounded by $N_s = 8$ pixels $(y_j)$. The CLCMB index is calculated for the blocks of each class $\omega_i$ as

$$CLCMB_{\omega_i,\omega_j} = \sum_{b=1}^{N_b}\sum_{s=1}^{N_s} \delta(\ell_c,\omega_i)\delta(\ell_s,\omega_j). \tag{6}$$

Here, $CLCMB_{\omega_i,\omega_j}$ is the CLCMB for class $\omega_i$ with class $\omega_j$. In this equation, $\ell_c$ is the class label of the central pixel of block $b$, and $\ell_s$ is the class label of its surrounding pixels $s$. The neighboring conditions in MRF say that: 1) a site cannot be a neighbor with itself $i \notin N'_i$; 2) the neighborhood relationship is mutual $(i \in N_j \iff j \in N_i)$ [10]. Therefore, the CLCMB is converted to the global class-label co-occurrence matrix of the blocks (GCLCMB), which is a square matrix of size $M$ and shows the global spatial frequency distribution of each pair of classes in the image, based on the selected blocks, i.e.,

$$GCLCMB_{\omega_i,\omega_j} = CLCMB_{\omega_i,\omega_j} + CLCMB_{\omega_j,\omega_i}. \tag{7}$$

The local posterior energy of the central pixel (1) is penalized by the frequency of the neighboring pixel labels as a spatial energy term (3). Thus, by globally analyzing an image, the probability that the true label $(\alpha)$ for a given pixel is misclassified as a false label $(\beta)$ due to the spatial energy is the same as the global joint probability distribution of each pair of those classes in the image, which is computed by GCLCMB. Therefore, $\psi_{\alpha\beta}$ for each pair of classes $(\psi_{\alpha\beta})$ is the element of the GCLCMB matrix, which belongs to classes $\alpha$ and $\beta$. In the next step, $\Delta U^l_{\alpha\beta}$ and $\psi_{\alpha\beta}$ are used to compute $\lambda_{\alpha\beta}$ for each pair of classes using (4). Finally, the average of $\lambda_{\alpha\beta}$ for all of the classes is computed and is called the optimized smoothing parameter $(\lambda^*)$, i.e.,

$$\lambda^* = \frac{\sum_{\alpha=1}^{M}\sum_{\beta=1}^{M}\lambda_{\alpha\beta}}{M(M-1)}. \tag{8}$$

### E. Edge Probability Map

Each image band may provide different or even conflicting information based on its wavelength. Hence, extraction of an accurate edge map for very high resolution multispectral images and hyperspectral images is a challenging topic [9], [13]. Therefore, a one-band gradient from the $B$-band image is computed by using the Canny edge detector for all bands $(B)$ and with $(n_t)$ hysteresis threshold levels between (0.1 and 1) [14]. By a summation for all bands and all threshold levels, the edge probability map is computed [15]. The resulting map is convolved with the Gaussian kernel to decrease the smoothness effects near boundary regions [14]. In order to relate the edge probability of each pixel to the smoothing parameter, a new spatially weighted parameter $w_{(i)}$ is constructed, i.e.,

$$w_{(i)} = 1 - \frac{1}{B \times n_t}\sum_{i=1}^{B}\sum_{j=1}^{n_t} G_{(i,j)}, \quad 0 < w_{(i)} \leq 1 \tag{9}$$

where $G_{(i,j)}$ is the binary edge map generated by using the Canny edge detector on each band at each hysteresis threshold. Therefore, to preserve the small structures and edges in the classified map, a new spatial energy component for edge for the adaptive MRF is proposed. Thus

$$U^E_{\text{spatial}}(y_i) = \sum_{y_j \in \mathbf{N}_i} w_{(i)}\left(1 - \delta(\ell_i,\ell_j)\right) \tag{10}$$

where superscript $E$ refers to the edge probability map.

## III. Results and Discussion

In order to evaluate the performance of the proposed smoothing parameter estimation method, several experiments were conducted using a multispectral satellite image, medium-resolution and very high resolution airborne hyperspectral images.

1) Mildura region image: A multispectral WorldView-2 (WV-2) image from 2010-05-21 comprising 521 × 521 pixels, which is located between 142.071 E, 34.188 S and 142.083 E, 34.197 S. The image of the area is very complex and comprises a variety of garden and building roof colors. Seven major land use and land cover types were chosen: gardens, farms, grass, trees, bare soil, roads, and buildings.
2) The Indian Pines image: A hyperspectral image of an agricultural area, which is recorded by the AVIRIS sensor. The image comprises 145 × 145 pixels with 20 m/pixel spatial resolution and 200 spectral bands. Its reference map contains 16 classes.

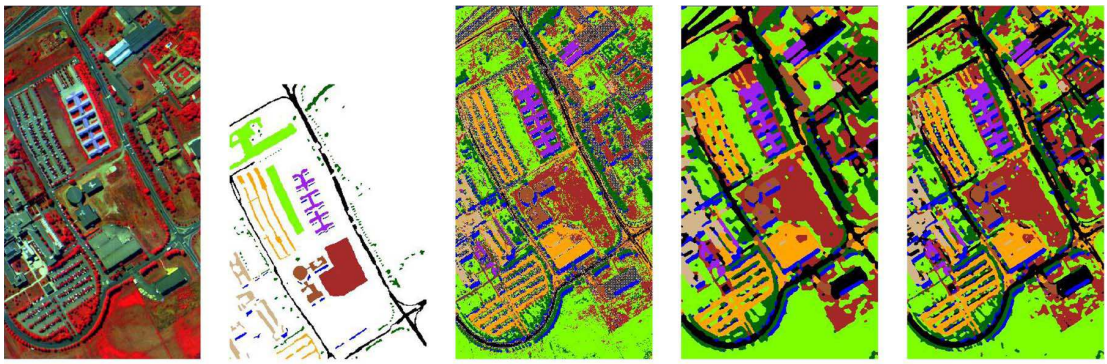

(a) (b) (c) (d) (e)

Fig. 3. University of Pavia. (a) Three-band color composite. (b) Reference data. (c) *SVM* pixelwise classification map. (d) *SVMMRF-NE* classification map. (e) *SVMMRF-E* classification map.

TABLE I
ESTIMATED $\lambda^*$ FOR *SVMMRF* METHODS

| Studying area | Mildura region | Indian pines | Pavia University |
|---|---|---|---|
| $\lambda^*$ | 0.913 | 0.9657 | 0.9605 |

3) The University of Pavia image: A very high spatial resolution hyperspectral image of an urban area, which is acquired by the ROSIS sensor comprises 610 × 340 pixels and 103 spectral channels [see Fig. 3(a)]. Nine classes of interest are considered [see Fig. 3(b)].

In order to compare the accuracy of classified maps, the same sets of test pixels for each image were selected by the stratified random method [16]. The training set contained 50 pixels per class, and the test set comprised 1000 pixels for all the classes for the WV-2 image. Table III gives the number of training and test pixels for each class for the AVIRIS and ROSIS data sets, respectively.

In this letter, multiclass one-versus-one SVM classification was adopted as a nonlinear classifier through the use of a Gaussian radial basis function kernel [9]. The optimal SVM parameters $C$ and $\gamma$ were chosen by fivefold cross validation [9]. The *SVMLIB* library was used to estimate the probability for individual classes for each pixel and produce the classification map [see Fig. 3(c)]. Then, the results of SVM classification were used to estimate smoothing parameter $\lambda^*$ for each data set (see Table I).

To estimate the efficiency of the parameter estimation method, we applied both nonedge-based SVMMRF and edge-based SVMMRF methods with different values of smoothing parameter $\lambda$, varying from 0.1 to 0.99. The resulting overall accuracy values for the three data sets are reported in Table II, from which it can be concluded that parameter $\lambda^*$ estimated by the proposed dynamic block-based method yielded the highest overall accuracy values for the three images.

Table III gives overall (OA), average (AA), and class-specific accuracy values, as well as the kappa coefficient (K) [7] for the SVM, *SVMMRF_NE*, and *SVMMRF_E* methods [9], for the Indian Pines and the University of Pavia images, respectively. Fig. 3(c)–(e) shows the corresponding classification maps for the University of Pavia image. It can be seen that the classification maps obtained by applying the MRF-based method with the optimal smoothing parameter contain more homogeneous regions and look less noisy than the SVM classification map.

TABLE II
OVERALL ACCURACY ASSESSMENT OF THE CLASSIFIED MAPS FOR *SVMMRF* METHOD WITH DIFFERENT SMOOTHING PARAMETERS AND *SVM* FOR *WV-2*, *AVIRIS*, AND *ROSIS* IMAGES

| Smoothing Parameter | Mildura region | | Indian pines | | Pavia University | |
|---|---|---|---|---|---|---|
| | $SVMMRF$ | | $SVMMRF$ | | $SVMMRF$ | |
| | $NE$ | $E$ | $NE$ | $E$ | $NE$ | $E$ |
| 0.1 | 73.9 | 74.5 | 87.8 | 85.5 | 85.3 | 85.2 |
| 0.2 | 73.8 | 74.9 | 89.1 | 87.7 | 87.4 | 86.9 |
| 0.3 | 73.8 | 76.5 | 90.5 | 89.1 | 88.6 | 85.9 |
| 0.4 | 74.2 | 76.8 | 90.9 | 90.3 | 89.2 | 89.2 |
| 0.5 | 74.5 | 77.7 | 91.1 | 90.3 | 89.6 | 89.5 |
| 0.6 | 74.7 | 77.4 | 91.6 | 91.0 | 90 | 89.9 |
| 0.7 | 75.2 | 77.5 | 91.6 | 92.0 | 90.4 | 90.4 |
| 0.8 | 76.8 | 78 | 91.6 | 92.1 | 91 | 91.7 |
| 0.9 | 77.4 | 78.8 | 91.6 | 92.2 | 91.4 | 93.9 |
| 0.99 | 76.3 | 76.2 | 91.3 | 91.7 | 84.8 | 92.1 |
| $\lambda^*$ | 77.7 | 82.5 | 91.8 | 92.3 | 91.5 | 94.1 |
| SVM | 73.5 | 73.5 | 82.2 | 82.2 | 84.8 | 84.8 |

We compared the performance of our classification system using the proposed smoothing parameter estimation method with the classification methods described in [9] and [17], which used similar data sets and methods. The results of this study indicate that the accuracy values obtained for the Indian Pines image are comparable with those obtained in previous works. However, the overall accuracy values of our method for the University of Pavia image are improved by 6.5% and 8.4%, when compared with the results of Tarabalka *et al.* [9], for *SVMMRF_E* and *SVMMRF_NE* methods, respectively.

The overall accuracy of the proposed *SVMMRF_E* framework is higher than that of the *SVMMRF_NE* method for all three data sets. We evaluated the statistical significance of the improvement of classification results in terms of accuracy, when the proposed edge probability index was included in the classification, by using McNemar's test with the 5% significance level for each pair of the classification maps of each data set [17]. According to the calculated $\chi^2$ and $z$ values, the null hypothesis $(H_0)$ of no significant difference between two map accuracy values is rejected for both Indian Pines and University of Pavia images. This means that the use of the proposed edge probability index is beneficial for MRF-based hyperspectral image classification. The results of the Pavia University and Indian Pines image classification were then compared with those of Tarabalka *et al.* [9]. Although using both fuzzy no-edge/edge index [9] and the edge probability map similarly increased

TABLE III
NUMBER OF TRAINING AND TEST PIXELS AND CLASSIFICATION ACCURACY IN PERCENTAGE FOR EACH CLASS OF **THE INDIAN PINES** IMAGE AND **THE UNIVERSITY OF PAVIA** IMAGE, WHERE **OA**, **AA**, AND **K** REPRESENT THE **OVERALL ACCURACY**, **AVERAGE ACCURACY**, AND **KAPPA COEFFICIENT**; CLASSES 1–9 IN THE UNIVERSITY OF PAVIA IMAGE REPRESENT ASPHALT, MEADOWS, GRAVEL, TREES, PAINTED METAL SHEETS, BARE SOIL, BITUMEN, SELF-BLOCKING BRICKS, AND SHADOWS, AND CLASSES 1–16 FOR THE INDIAN PINES IMAGE REPRESENT ALFALFA, CORN-NO TILL, CORN-MIN TILL, CORN, GRASS/PASTURE, GRASS TREES, GRASS/PASTURE-MOWED, HAY-WINDROWED, OATS, SOYBEANS-NO TILL, SOYBEANS-MIN TILL, SOYBEANS-CLEAN TILL, WHEAT, WOODS, BLDF-GRASS-TREE-DRIVES, STON-STEEL TOWERS, RESPECTIVELY

| | **The University of Pavia** | | | | | **The Indian pines** | | | | |
|---|---|---|---|---|---|---|---|---|---|---|
| | No. of samp | | $SVM$ | $SVMMRF$ | | No. of samp | | $SVM$ | $SVMMRF$ | |
| | Train | Test | | $NE$ | $E$ | Train | Test | | $NE$ | $E$ |
| OA | - | - | 84.8 | 91.5 | 94.1 | - | - | 82.2 | 91.8 | 92.3 |
| AA | - | - | 88.0 | 93.1 | 94.3 | - | - | 85.1 | 95.3 | 95.7 |
| K | - | - | 0.803 | 0.892 | 0.922 | - | - | 0.797 | 0.905 | 0.912 |
| 1 | 50 | 6581 | 71.7 | 83.9 | 82.5 | 15 | 39 | 63.0 | 85.2 | 85.2 |
| 2 | 50 | 18599 | 86.4 | 93.1 | 97.5 | 100 | 1334 | 75.3 | 88.8 | 89.0 |
| 3 | 50 | 2049 | 74.8 | 81.9 | 83.4 | 100 | 734 | 70.8 | 79.8 | 84.2 |
| 4 | 50 | 3014 | 93.1 | 93.6 | 93.9 | 100 | 134 | 95.0 | 99.4 | 99.4 |
| 5 | 50 | 1295 | 99.2 | 99.7 | 98.6 | 100 | 397 | 96.4 | 97.4 | 98.1 |
| 6 | 50 | 4979 | 82.5 | 91.2 | 93.5 | 100 | 647 | 97.2 | 99.6 | 100 |
| 7 | 50 | 1280 | 95.6 | 98.4 | 100.0 | 15 | 11 | 92.3 | 100 | 100 |
| 8 | 50 | 3632 | 90.1 | 96.9 | 99.4 | 100 | 389 | 99.5 | 99.8 | 99.8 |
| 9 | 50 | 897 | 99.0 | 99.1 | 99.9 | 15 | 5 | 100 | 100 | 100.0 |
| 10 | - | - | - | - | - | 100 | 868 | 88.8 | 98.3 | 98.7 |
| 11 | - | - | - | - | - | 100 | 2368 | 69.4 | 85.0 | 84.7 |
| 12 | - | - | - | - | - | 100 | 514 | 88.5 | 98.5 | 98.5 |
| 13 | - | - | - | - | - | 100 | 112 | 99.3 | 99.3 | 99.3 |
| 14 | - | - | - | - | - | 100 | 1194 | 91.5 | 95.2 | 96.3 |
| 15 | - | - | - | - | - | 100 | 280 | 83.6 | 98.4 | 98.7 |
| 16 | - | - | - | - | - | 50 | 45 | 100 | 100 | 100 |

the *SVMMRF_E* classification accuracy for the Pavia University data set, a comparison of the two results reveals that the proposed edge probability map improved the overall accuracy by 2.6% (see Table II), while the use of the fuzzy no-edge/edge index in [9] improved the overall accuracy by only 0.7%. For the Indian Pines image, the use of no-edge/edge index in [9] yielded a decrease in overall accuracy of 0.2%, while the proposed edge probability map yielded the improvement of overall accuracy by 0.5%.

This nonsignificant difference between the *SVMMRF_E* and *SVMMRF_NE* classification maps of the Mildura image needs to be interpreted with caution. Because this image contains large spatial structures, the selected test points do not comprise region edges due to the small subpopulation of the region edge pixels in the image.

## IV. CONCLUSION

In this letter, a novel robust framework for the smoothing parameter estimation for the spectral–spatial classification of very high spectral and spatial resolution remote sensing images has been presented. This method consists in performing SVM classification, followed by a new concept that is called dynamic blocks and two new indexes (CLCMB and GCLCMB) to estimate the smoothing parameter for MRF-based optimization. Furthermore, a new spatially weighted parameter based on the Canny filter is proposed, which helps in preserving edges in the image scene. Experimental results have demonstrated that the proposed method can estimate the optimal smoothing parameter, and it yields accurate classification maps for images captured by different types of sensors.

## ACKNOWLEDGMENT

The authors would like to thank DigitalGlobe for providing the DigitalGlobe WorldView-2 images, the Murray-Darling Basin Authority for providing the very high resolution aerial images, and the anonymous reviewers for comments that helped improve and clarify this manuscript.

## REFERENCES

[1] M. J. Duggin and C. J. Robinove, "Assumptions implicit in remote sensing data acquisition and analysis," *Int. J. Remote Sens.*, vol. 11, no. 10, pp. 1669–1694, 1990.

[2] X. Li, Y. Du, and F. Ling, "Spatially adaptive smoothing parameter selection for Markov random field based sub-pixel mapping of remotely sensed images," *Int. J. Remote Sens.*, vol. 33, no. 24, pp. 7886–7901, 2012.

[3] H. Derin and H. Elliott, "Modeling and segmentation of noisy and textured images using Gibbs random fields," *IEEE Trans. Pattern Anal. Mach. Intell.*, vol. PAMI-9, no. 1, pp. 39–55, Jan. 1987.

[4] F. Salzenstein and W. Pieczynski, "Parameter estimation in hidden fuzzy Markov random fields and image segmentation," *Graph. Models Image Process.*, vol. 59, no. 4, pp. 205–220, Jul. 1997.

[5] B. C. Tso and P. M. Mather, "Classification of multisource remote sensing imagery using a genetic algorithm and Markov random fields," *IEEE Trans. Geosci. Remote Sens.*, vol. 37, no. 3, pp. 1255–1260, May 1999.

[6] S. B. Serpico and G. Moser, "Weight parameter optimization by the Ho–Kashyap algorithm in MRF models for supervised image classification," *IEEE Trans. Geosci. Remote Sens.*, vol. 44, no. 12, pp. 3695–3705, Dec. 2006.

[7] X. Jia and J. Richards, "Managing the spectral–spatial mix in context classification using Markov random fields," *IEEE Geosci. Remote Sens. Lett.*, vol. 5, no. 2, pp. 311–314, Apr. 2008.

[8] V. A. Tolpekin and A. Stein, "Quantification of the effects of land-cover-class spectral separability on the accuracy of MRF-based superresolution mapping," *IEEE Trans. Geosci. Remote Sens.*, vol. 47, no. 9, pp. 3283–3297, Sep. 2009.

[9] Y. Tarabalka, M. Fauvel, J. Chanussot, and J. A. Benediktsson, "SVM- and MRF-based method for accurate classification of hyperspectral images," *IEEE Geosci. Remote Sens. Lett.*, vol. 7, no. 4, pp. 736–740, Oct. 2010.

[10] E. Levitan and G. Herman, "A maximum a posteriori probability expectation maximization algorithm for image reconstruction in emission tomography," *IEEE Trans. Med. Imag.*, vol. 6, no. 3, pp. 185–192, Sep. 1987.

[11] H. Aghighi and J. Trinder, "Smoothing parameter estimation framework for Markov random field by using contextual and spectral information," in *Proc. SPIE Remote Sens.*, 2013, pp. 88920T-1–88920T-10.

[12] S. K. Sengupta, C. Kamath, D. N. Poland, and J. A. Futterman, "Detecting human settlements in satellite images," in *Proc. High-Power Lasers Appl.*, pp. 76–83, Society for Optics and Photonics.

[13] S. Giannarou and T. Stathaki, "Optimal edge detection using multiple operators for image understanding," *EURASIP J. Adv. Signal Process.*, vol. 2011, no. 1, pp. 1–19, 2011.

[14] S. Candemir and Y. S. Akgl, *Adaptive Regularization Parameter for Graph Cut Segmentation*. New York, NY, USA: Springer-Verlag, 2010, pp. 117–126.

[15] M. Hedley and H. Yan, "Segmentation of color images using spatial and color space information," *J. Electron. Imag.*, vol. 1, no. 4, pp. 374–380, 1992.

[16] G. M. Foody, "Thematic map comparison: Evaluating the statistical significance of differences in classification accuracy," *Photogramm. Eng. Remote Sens.*, vol. 70, no. 5, pp. 627–633, 2004.

[17] B. Zhang, S. Li, X. Jia, L. Gao, and M. Peng, "Adaptive Markov random field approach for classification of hyperspectral imagery," *IEEE Geosci. Remote Sens. Lett.*, vol. 8, no. 5, pp. 973–977, Sep. 2011.